Chemistry–A European Journal

Supporting Information

π-Extended Donor–Acceptor Porphyrins and Metalloporphyrins for Antimicrobial Photodynamic Inactivation

Anzhela Galstyan,*[a] Yogesh Kumar Maurya,[b] Halina Zhylitskaya,[b] Youn Jue Bae,[c] Yi-Lin Wu,[c, e] Michael R. Wasielewski,*[c] Tadeusz Lis,[b] Ulrich Dobrindt,[d] and Marcin Stępień*[b]

Supporting Information

Table of Contents

General: Dichloromethane was distilled from calcium hydride. All other solvents and reagents were used as received**.** Compound **1**, **H_2-NDP** and **Zn-NDP** were synthesized as previously described.[1] ^{1}H NMR spectra were recorded on high-field spectrometer (^{1}H frequency 500.13 MHz), equipped with broadband inverse gradient probeheads. Spectra were referenced to the residual solvent signals (chloroform-*d*, 7.24 ppm). ^{13}C NMR spectra were recorded with ^{1}H broadband decoupling and referenced to solvent signals ($^{13}CDCl_3$, 77.0 ppm). High resolution mass spectra were recorded using ESI or MALDI ionization in the positive mode.

Dynamic light scattering (DLS). Dynamic light scattering was performed using a Nano ZS-90 apparatus utilizing a 633 nm red laser beam (at 90° angle) from Malvern Instruments to find the size and dispersity of nanospheres of PSs. The average size values reported are based on an average of three consecutive measurements.

Transient absorption spectroscopy and global analysis. Femtosecond transient absorption spectroscopy (fsTA) was performed using a regeneratively amplified Ti:sapphire laser system operating at 1kHz to generate 828 nm. The frequency-doubled 414 nm light is used to pump a lab built optical parametric amplifier to generate tunable pump wavelengths of 600 nm, 580 nm and 540 nm for **H_2-**, **Zn-**, and **Pd-NDP** respectively.[2] Solution samples were prepared in 2 mm path length glass cuvettes and degassed with three freeze-pump-thaw cycles. Two different time windows of 7.4 ns and 340 μs are used to capture the entire dynamics using commercial spectrometers (customized Ultrafast Systems, LLC Helious and EOS spectrometers for 7.4 ns and 340 μs time windows, respectively). The TA data were subjected to global kinetic analysis to obtain the evolution- and decay-associated spectra and kinetic parameters as described in detail previously.[3]

Computational methods. Density functional theory (DFT) calculations were performed using Gaussian 09.[4] In each case, DFT geometries were refined to meet standard convergence criteria, and the existence of a stationary point was verified by a normal mode frequency calculation. Geometry optimizations, frequency calculations, and thermochemistry calculations were performed using the hybrid functional B3LYP[5–7]combined with the 6-31G(d,p) and sdd (for **Pd**) basis set. In the calculations of absorption spectra, up to 30 electronic transitions were calculated by means of time-dependent DFT (TD-DFT), using the above level of theory.

X-ray crystallography. X-ray quality crystals were grown by slow diffusion of water into a ethyl acetate solution of **Pd-NDP**. Diffraction measurements were performed on a κ geometry XCALIBUR diffractometer (ω scans), equipped with an ONYX CCD camera, with graphite monochromatized Cu K_α radiation. The data for **Pd-NDP** were collected at 100 K, corrected for Lorenz and polarization effects. Data collection, cell refinement, data reduction and analysis were carried out with the Xcalibur PX software, CRYSALIS CCD and CRYSALIS RED, respectively (Oxford Diffraction Ltd., Abignon, England, 2009). The structure was solved by direct methods with the SHELXS-2013 program and refined using SHELXL-2013 with anisotropic thermal parameters for non-H atoms. In the final refinement cycles, all H atoms were treated as riding atoms in geometrically optimized positions. CCDC 1935942 contains the supplementary crystallographic data for this paper. These data can be obtained free of charge from the Cambridge Crystallographic Data Centre via www.ccdc.cam.ac.uk/data_request/cif.

1. Synthesis

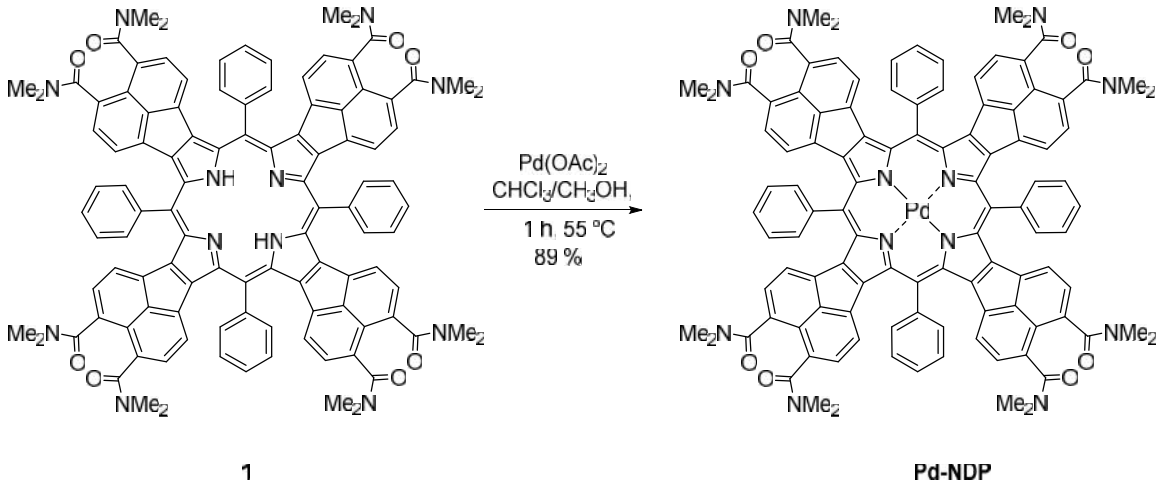

Scheme S1. Synthesis of Pd-complex, **Pd-NDP**.

5,10,15,20-Tetraphenyltetra(N,N,N',N'-tetramethylacenaphtho-5,6-dicarboxamide) [1,2-b:1',2'-g:1'',2''-l:1''',2'''-q]porphyrinato palladium(II) (Pd-NDP). A palladium acetate (13.37 mg, 0.06 mmol) solution in $CHCl_3/CH_3OH$ (2mL, 1/1) was added to the solution of compound **1** (20 mg, 0.012 mmol) in $CHCl_3$ (10 mL) and the resulting mixture was stirred at 55 for 1 h. TLC shows the complete consumption of starting material. The reaction mixture was diluted with dichloromethane, washed with water and brine, and dried over anhydrous sodium sulfate. The solvent was evaporated and the crude product was passed through a very short (about 5-6 cm) alumina column in order to get rid of palladium salt. The solvent was evaporated on rotary evaporator and the precipitate was crystallized using dichloromethane/hexane solvent to give product as a violet powder (18.94 mg, 89%). ^{1}H NMR (500 MHz, chloroform-*d*, 300 K): δ 2.72 (12H, s), 3.01 (12H, s), 3.02 (12H, s), 3.05 (12H, s), 5.47 (8H, m), 6.99 (8H, m), 7.87 (8H, m), 7.96 (4H, m), 8.67 (8H, m). ^{13}C NMR (125 MHz, chloroform-*d*, 300 K): δ 34.72, 34.85, 39.38, 39.56, 123.17, 123.57, 124.73, 126.64, 126.82, 130.07, 130.35, 130.66, 134.40, 134.50, 134.64, 135.16, 136.76, 136.89, 141.57, 141.98, 145.58, 145.76, 170.6. HRMS (MALDI–TOF): *m/z*: $[M]^+$ Calcd for $C_{108}H_{84}N_{12}O_8Pd$: 1782.558; Found 1782.532. UV-vis (CH_2Cl_2, 300 K) λ [nm] (ε in M^{-1} cm^{-1}): 380 (42 000), 541 (196 000), 633 (44 000), 679 (39 000).

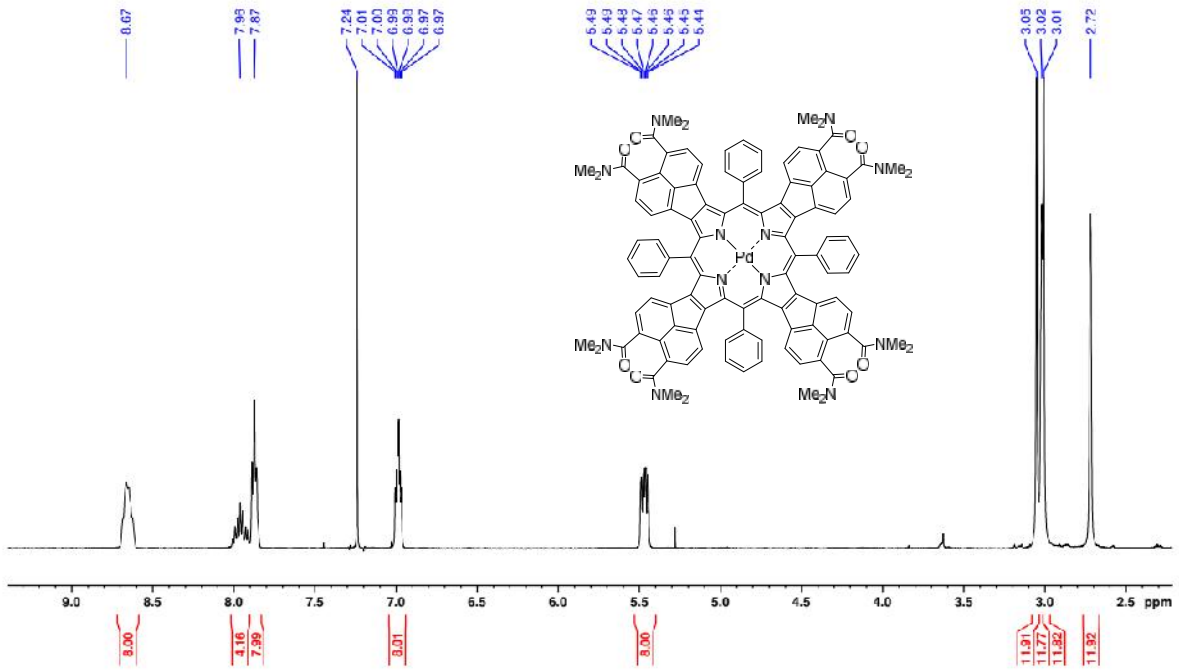

Figure S1. ^{1}H NMR spectrum of **Pd-NDP** (500 MHz, chloroform-*d*, 300 K).

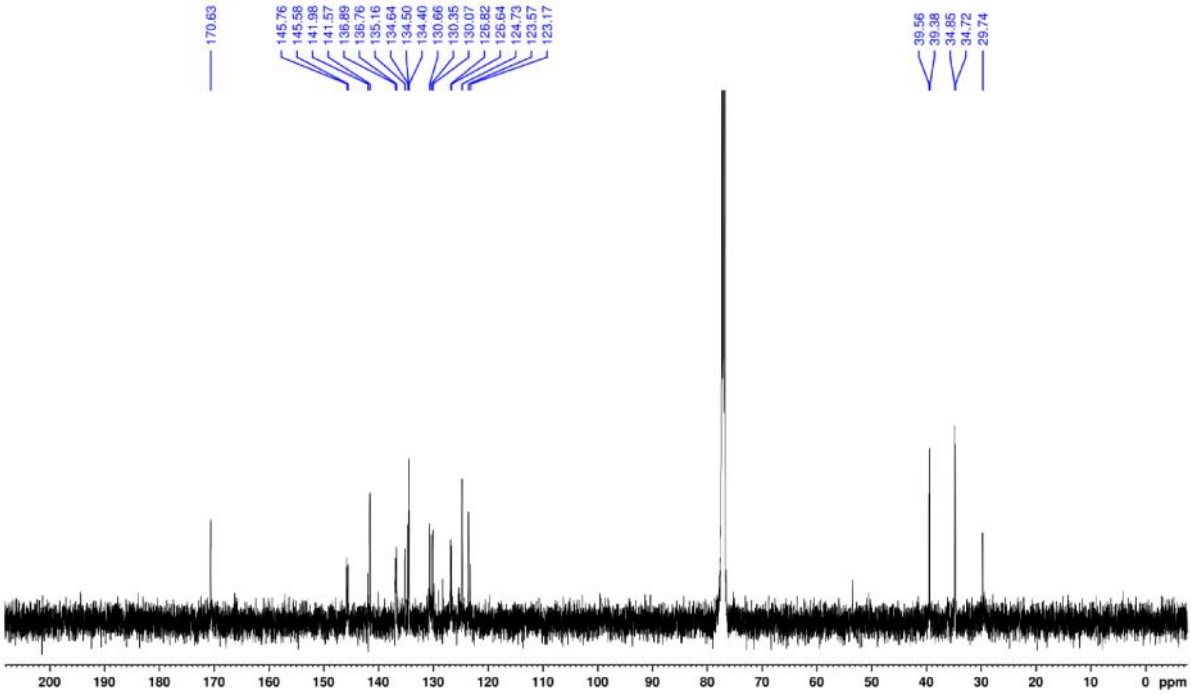

Figure S2. ^{13}C NMR spectrum of **Pd-NDP** (125 MHz, chloroform-*d*, 300 K).

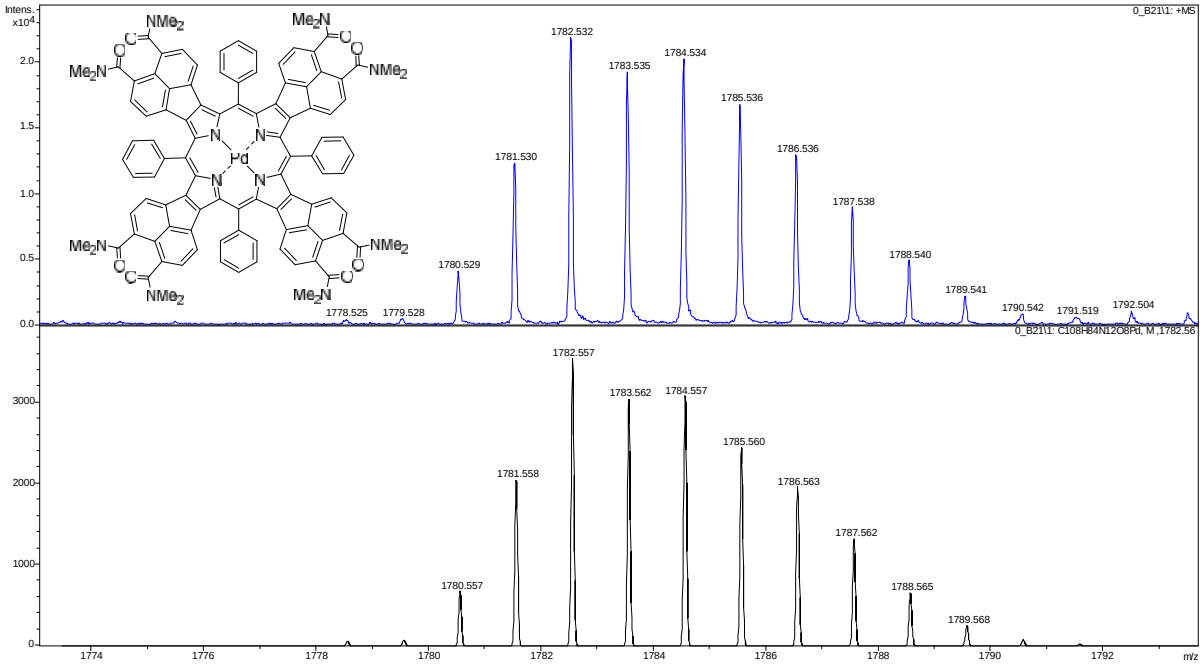

Figure S3. High resolution mass spectrum of **Pd-NDP** (MALDI–TOF, top: experimental, bottom: simulated).

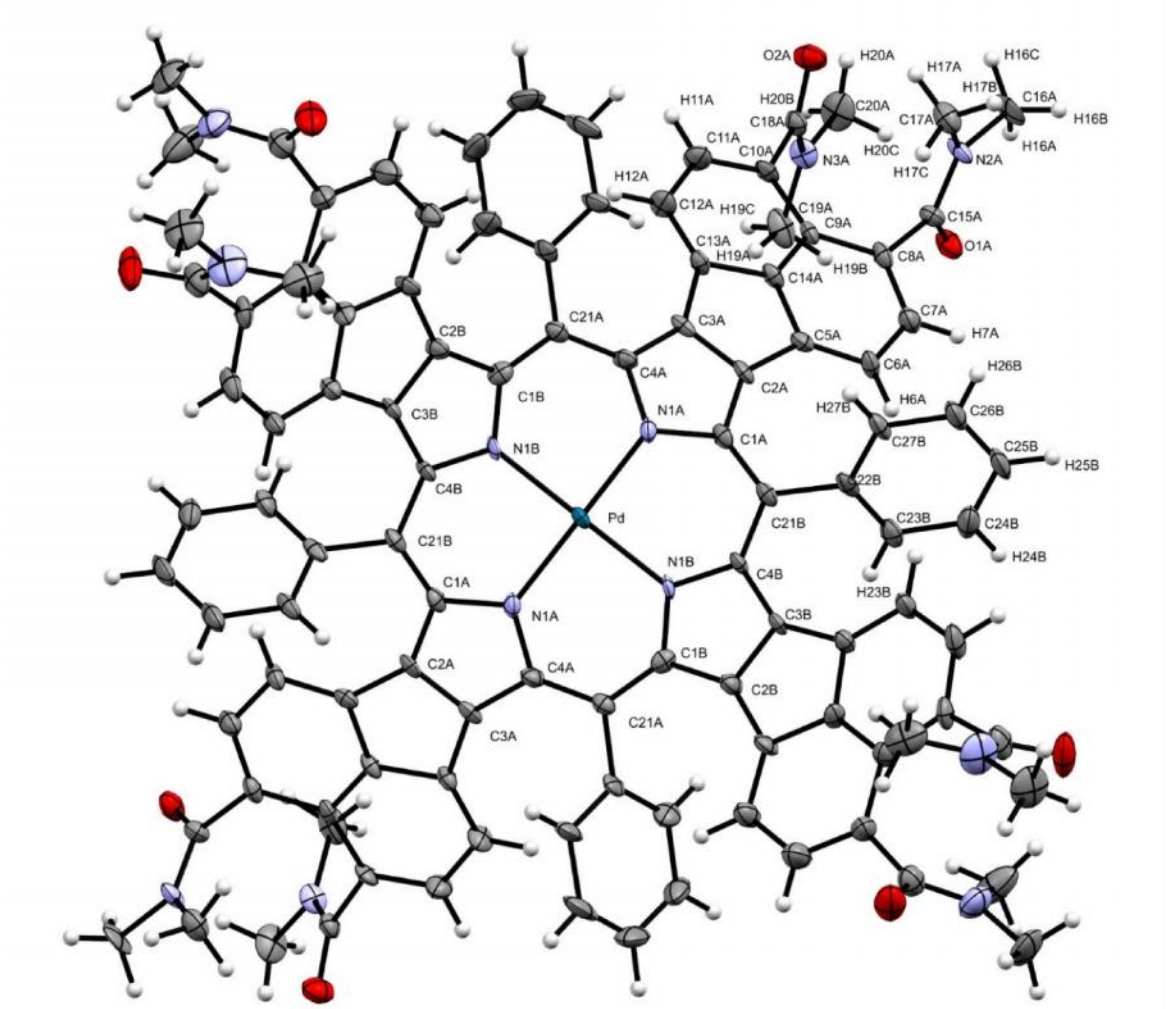

Figure S4. X-ray crystal structure of **Pd-NDP**.4($C_4H_8O_2$).H_2O. Solvent molecules are removed for clarity.

Table S1. Crystal data and structure refinement for **Pd-NDP**.4($C_4H_8O_2$).H_2O.

Identification code	ymo16a	
Empirical formula	C124 H118 N12 O17 Pd	
Formula weight	2154.70	
Temperature	100(2) K	
Wavelength	1.54184 Å	
Crystal system	Orthorhombic	
Space group	Fdd2	
Unit cell dimensions	a = 69.30(2) Å	α= 90°.
	b = 41.669(11) Å	β= 90°.
	c = 7.574(2) Å	γ = 90°.
Volume	21871(10) $Å^3$	
Z	8	
Density (calculated)	1.309 Mg/m^3	
Absorption coefficient	1.963 mm^{-1}	
F(000)	9024	
Crystal size	0.160 x 0.016 x 0.004 mm^3	
Theta range for data collection	4.244 to 68.004°.	
Index ranges	-82<=h<=78, -40<=k<=49, -6<=l<=8	
Reflections collected	11730	
Independent reflections	6776 [R(int) = 0.0758]	
Completeness to theta = 66.500°	98.1 %	
Absorption correction	Analytical	
Max. and min. transmission	0.994 and 0.903	
Refinement method	Full-matrix least-squares on F^2	
Data / restraints / parameters	6776 / 61 / 749	
Goodness-of-fit on F^2	1.073	
Final R indices [I>2sigma(I)]	R1 = 0.0675, wR2 = 0.1524	
R indices (all data)	R1 = 0.0897, wR2 = 0.1662	
Absolute structure parameter	-0.007(13)	
Extinction coefficient	n/a	
Largest diff. peak and hole	0.945 and -0.574 e.$Å^{-3}$	

2. Photophysical Data

Table S2. Photophysical data for H_2-**NDP,** Zn-**NDP**, and Pd-**NDP**.

PS	log$P_{o/w}$[a]	Solvent	λ_{abs}/nm ($\log_{10}\varepsilon$)	Φ_Δ[b]	Triplet states[c]		
					λ_{ex}/nm	$\tau_{S\rightarrow T}$ ps[d]	$\tau_{T\rightarrow GS}$ µs[e]
H_2-**NDP**	0.31	DCM	410 (4.72), 566 (5.29), 646 (4.36), 716 (4.16)	0.59	600	605 ± 2	54 ± 1[f]
		H_2O	414 (4.61), 583 (5.02), 724 (4.12)	0.50			
Zn-**NDP**	0.32	DCM	416 (4.81), 581 (5.36), 702 (4.45), 792 (4.14)	0.57	580	530 ± 10	77 ± 1
		H_2O	424 (4.70), 594 (5.04), 714 (4.36)	0.07			
Pd-**NDP**	0.51	DCM	380 (4.62), 541 (5.30), 633 (4.64), 679 (4.59)	1.00	540	2.6 ± 0.1	20 ± 1
		H_2O	386 (4.61), 544 (5.05), 641 (4.56), 687 (4.44)	0.39			

[a] 1-Octanol/water partition coefficient. [b] Quantum yields of singlet oxygen photogeneration measured using the relative method and methylene blue as a reference. Estimated accuracy ± 0.03. [c] Triplet formation and decay (deoxygenated dichloromethane, excitation at λ_{ex}). [d] Singlet (S) to triplet (T) intersystem crossing. [e] Decay of triplet (T) to the ground state (GS). [f] the major component of a biexponential decay.

2.1 Absorption spectra

Absorption spectra were measured on Agilent 8453 spectrophotometer and baseline corrected. Steady-state emission spectra were recorded on a HORIBA Jobin-Yvon IBH FL-322 Fluorolog 3 spectrometer equipped with a 450 W xenon-arc lamp, double-grating excitation and emission monochromators (2.1 nm/mm dispersion; 1200 grooves/mm). All solvents used were of the spectrometric grade. All experiments were performed at room temperature.

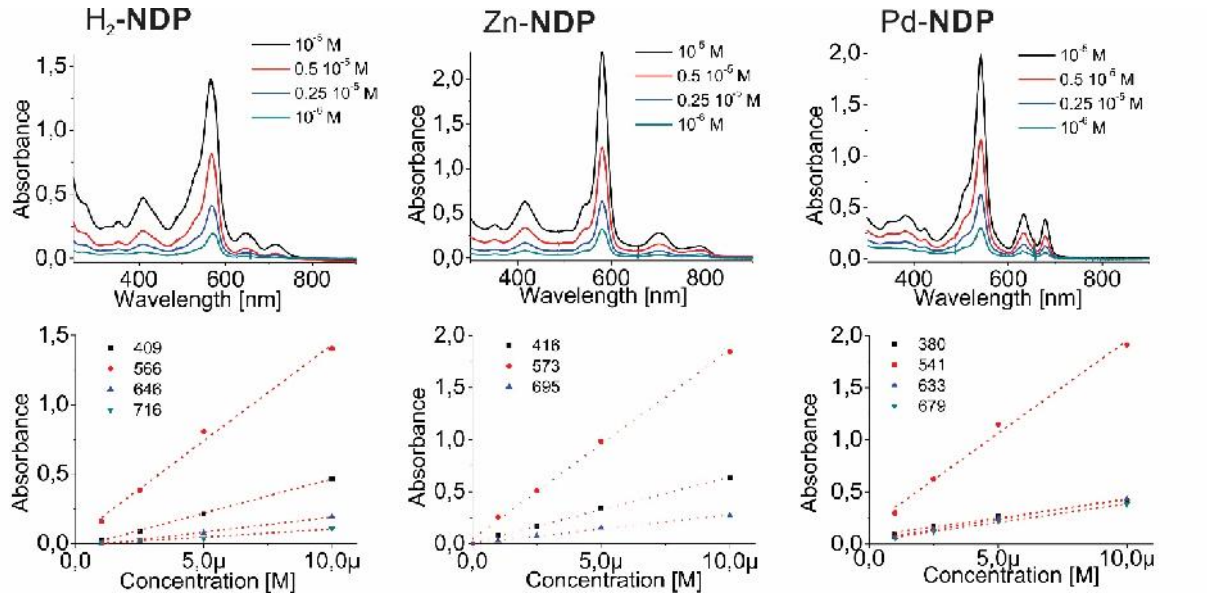

Figure S5. UV-Visible spectra of H_2-**NDP**, Zn-**NDP** and Pd-**NDP** in CH_2Cl_2 at different concentrations 1μM to 10μM and plots of the absorbance vs the concentration of the photosensitizer (the line represents the best-fitted straight line).

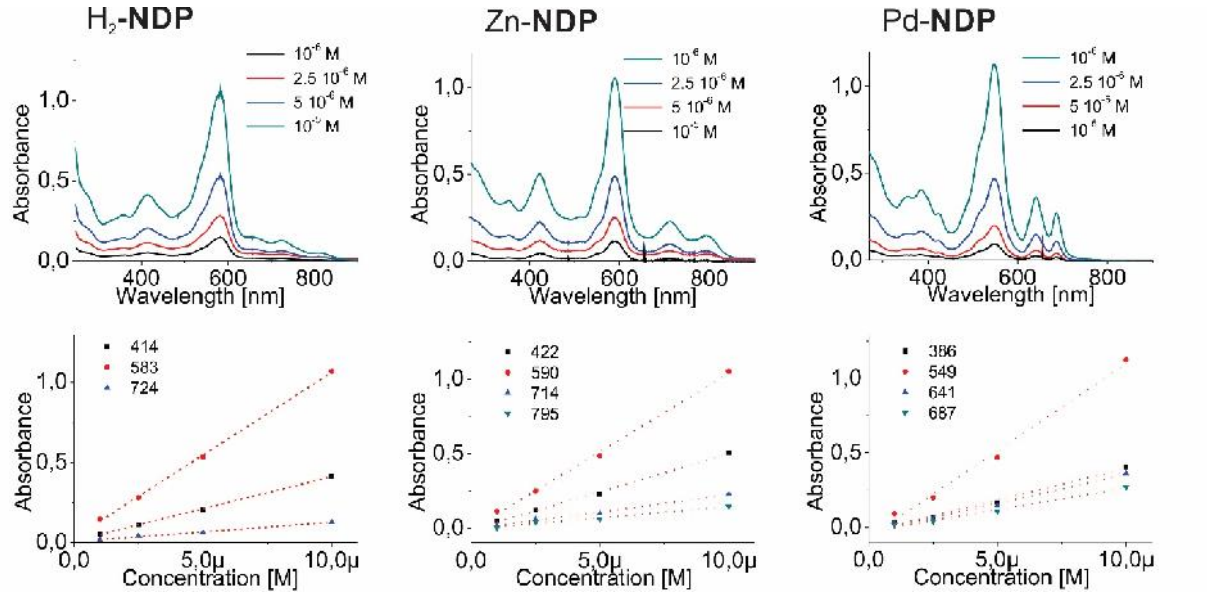

Figure S6. UV-Visible spectra of H_2-**NDP**, Zn-**NDP** and Pd-**NDP** in H_2O at different concentrations 1μM to 10μM and plots of the absorbance vs the concentration of the photosensitizer (the line represents the best-fitted straight line).

2.2 Singlet molecular oxygen quantum yields

Singlet oxygen quantum yields were determined using the relative method. Polychromatic irradiation from a projector lamp passing through a cut-off filter at 515 nm was used to carry out the experiments. Freshly prepared dye solution in dark flasks were mixed with the PSs only immediately before taking the samples at "0 time." $^1O_2$ photogeneration rates in DCM were derived using 1,3-diphenylisobenzofuran (DPBF). The initial absorbance of DPBF was adjusted to about 1.0, then the PS was added to reach absorbance about 0.2-0.3. The photooxidation of DPBF was monitored between 0 s to 25 s. $^1O_2$ photogeneration rates in water were derived using 9,10-anthracenediyl-*bis*(methylene)dimalonic acid (ABMDMA) as a fluorescent monitor for photosensitized bleaching rates monitored between 0 s to 60 s. The c_Δ for the samples was calculated according to the following equation:

$$\Phi_\Delta^S = \Phi_\Delta^R \cdot \frac{r_S}{r_R} \cdot \frac{\int_{\lambda 1}^{\lambda 2} I_0(\lambda) \cdot (1-10^{-A_R(\lambda)}) \cdot d\lambda}{\int_{\lambda 1}^{\lambda 2} I_0(\lambda) \cdot (1-10^{-A_S(\lambda)}) \cdot d\lambda}$$

where r is the slope of the monitor's bleaching over time (plotted as ln (A_0/A) for DPBF and as emission intensity integral for ABMDMA), $\lambda_1 - \lambda_2$ is the irradiation wavelength interval, $I_0(\lambda)$ the incident spectral photon flow, $A(\lambda)$the absorbance, and the subscripts R and S are the reference (methylene blue, c_Δ = 0.53 in DCM and c_Δ = 0.52 in H_2O) and sample, respectively. The incident intensity can be approximated by a constant value, drawn out of the integral and canceled.

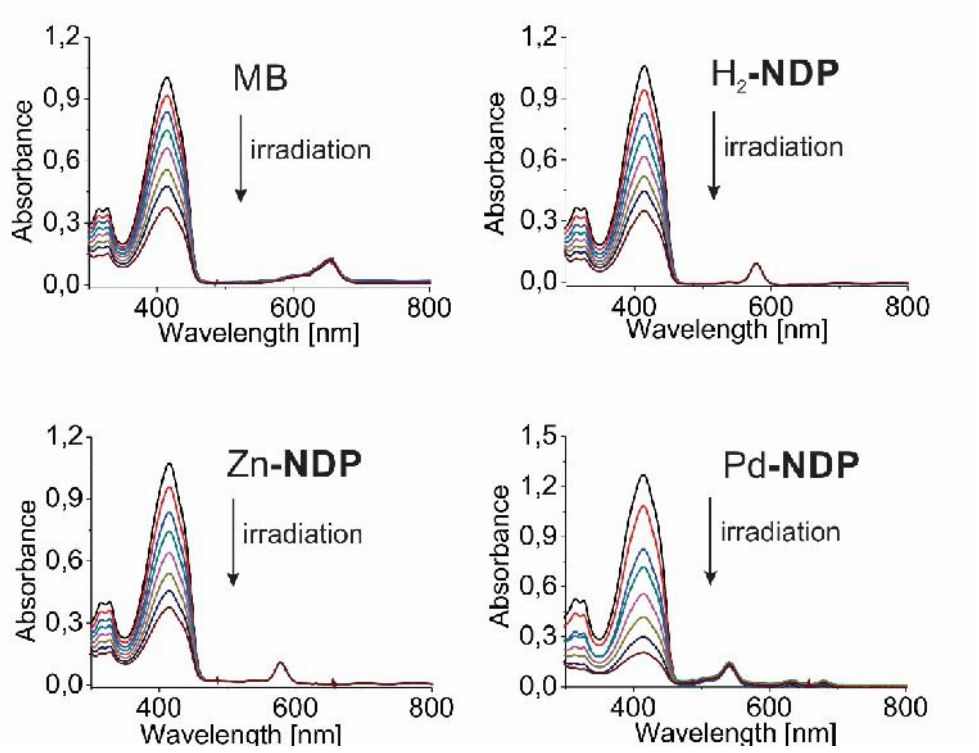

Figure S7. Time-dependent decomposition of DPBF photosensitized by **H_2-NDP**, **Zn-NDP** and **Pd-NDP** in DCM upon irradiation with light from projector lamp filtered through a cut-off filter λ > 515 nm.

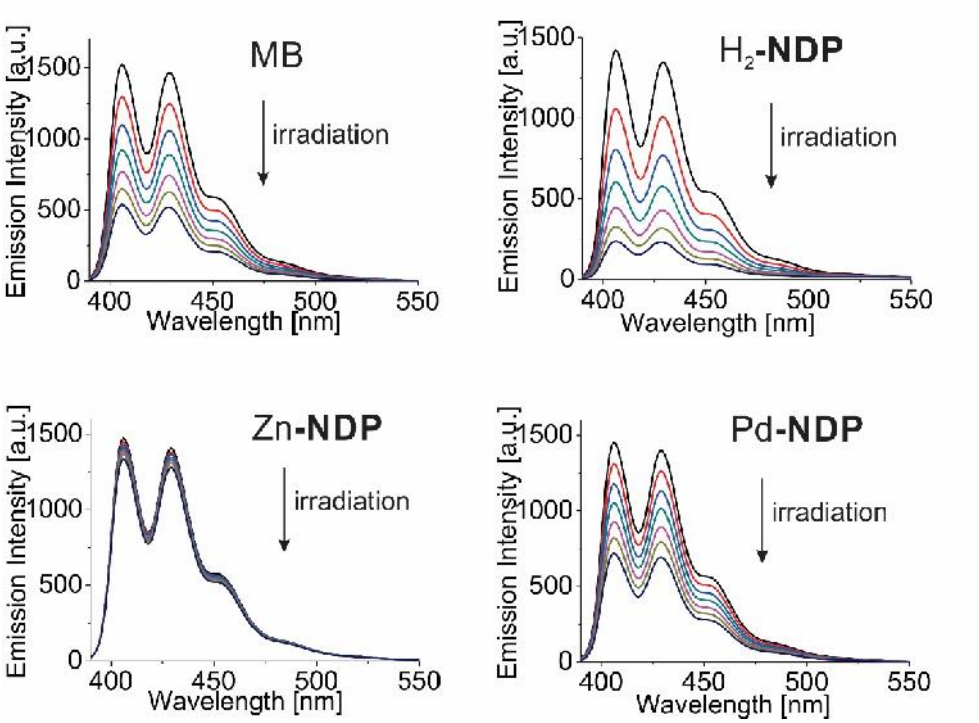

Figure S8. Time-dependent decomposition of ABMDMA photosensitized by **H_2-NDP**, **Zn-NDP** and **Pd-NDP** in H_2O upon irradiation with light from projector lamp filtered through a cut-off filter λ > 515 nm..

2.3 Partition Coefficients

1-Octanol/water partition coefficients (log$P_{o/w}$) were determined at 25°C using equal volumes of water (1 mL) and 1-octanol (1 mL). The final concentration of compound was approx. 25 μM. The mixture was stirred for 1h and centrifuged (10 min, 4400 rpm) to enable a phase separation. An aliquot (50 μL) of aqueous and organic phases were dissolved in 1 mL of *N*,*N*-dimethylformamide (DMF) and final concentration determined by absorption spectroscopy. log$P_{o/w}$ was calculated according to the following equation:

Log$P_{o/w}$ = Log ([PS]octanol / [PS]water)

2.4 DLS measurements

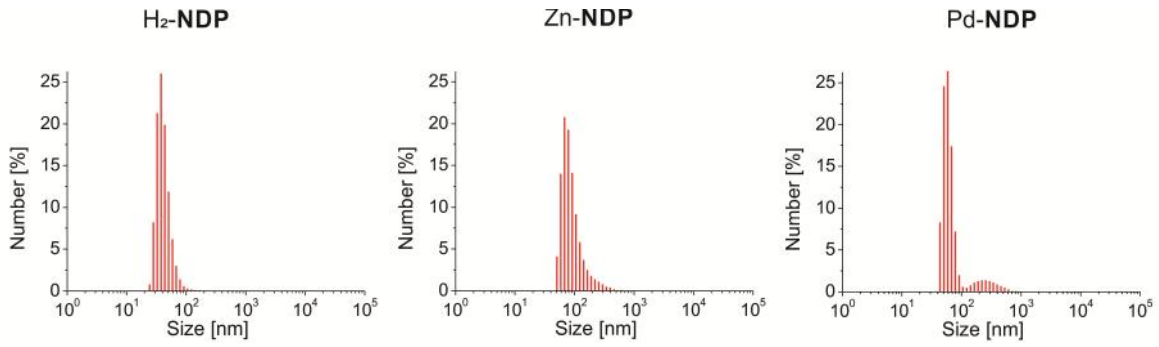

***Figure S9**. Hydrodynamic distribution of NDPs in water.*

2.4 Triplet State Lifetimes

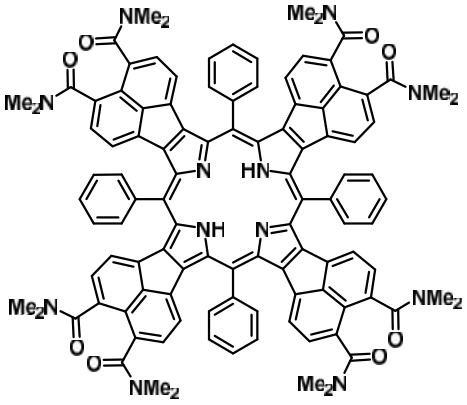

H_2-NDP

H_2–NDP.

Upon photoexcitation of **H_2-NDP** in DCM using 600 nm (1 μJ/pulse), there is singlet excited state absorption (ESA) that spans from 380 nm to 1600 nm. In later time, there is triplet formation where the spectral feature is similar to singlet ESA except in the 1300 nm region (Figure S9a). The effective singlet decay time constant (605 ± 2 ps) is obtained by globally fitting the fsTA spectra using A → B → GS where A is the singlet and B is the triplet. The triplet decay is measured using time window of 340 μs (Figure S10). Using the tri-exponential fit, the singlet decays within the instrument response function (IRF) and triplet decays bi-exponentially with time constants of 54 ± 1 μs and 210 ± 10 μs.

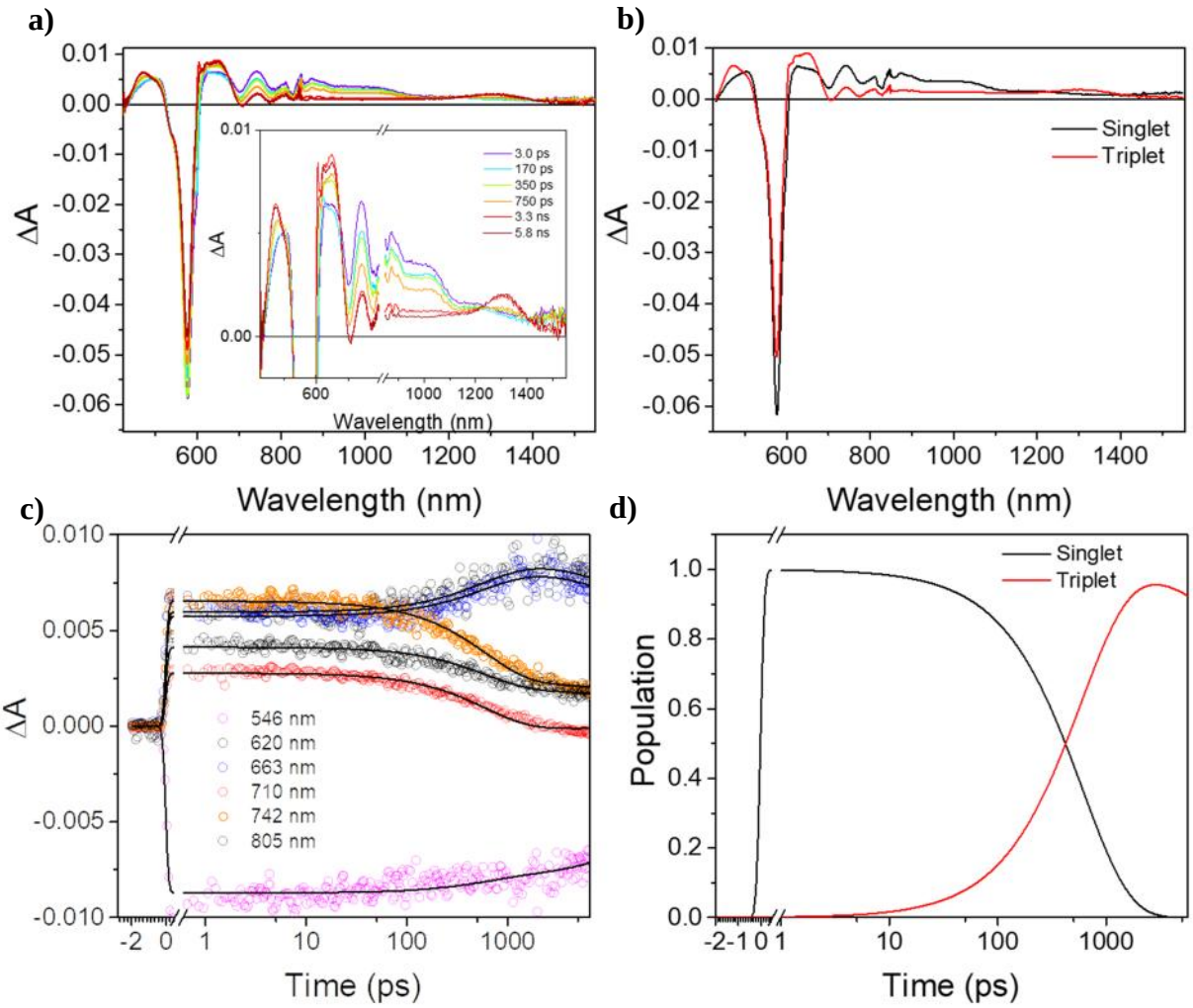

Figure S10. (a) fsTA spectra of H_2-**NDP** at selected time points with the inset showing the excited state abosorption features. (b) species-associated spectra using the kinetic model A → B → GS where A is singlet and B is triplet. (c) wavelength fitting and (d) population vs. time plots.

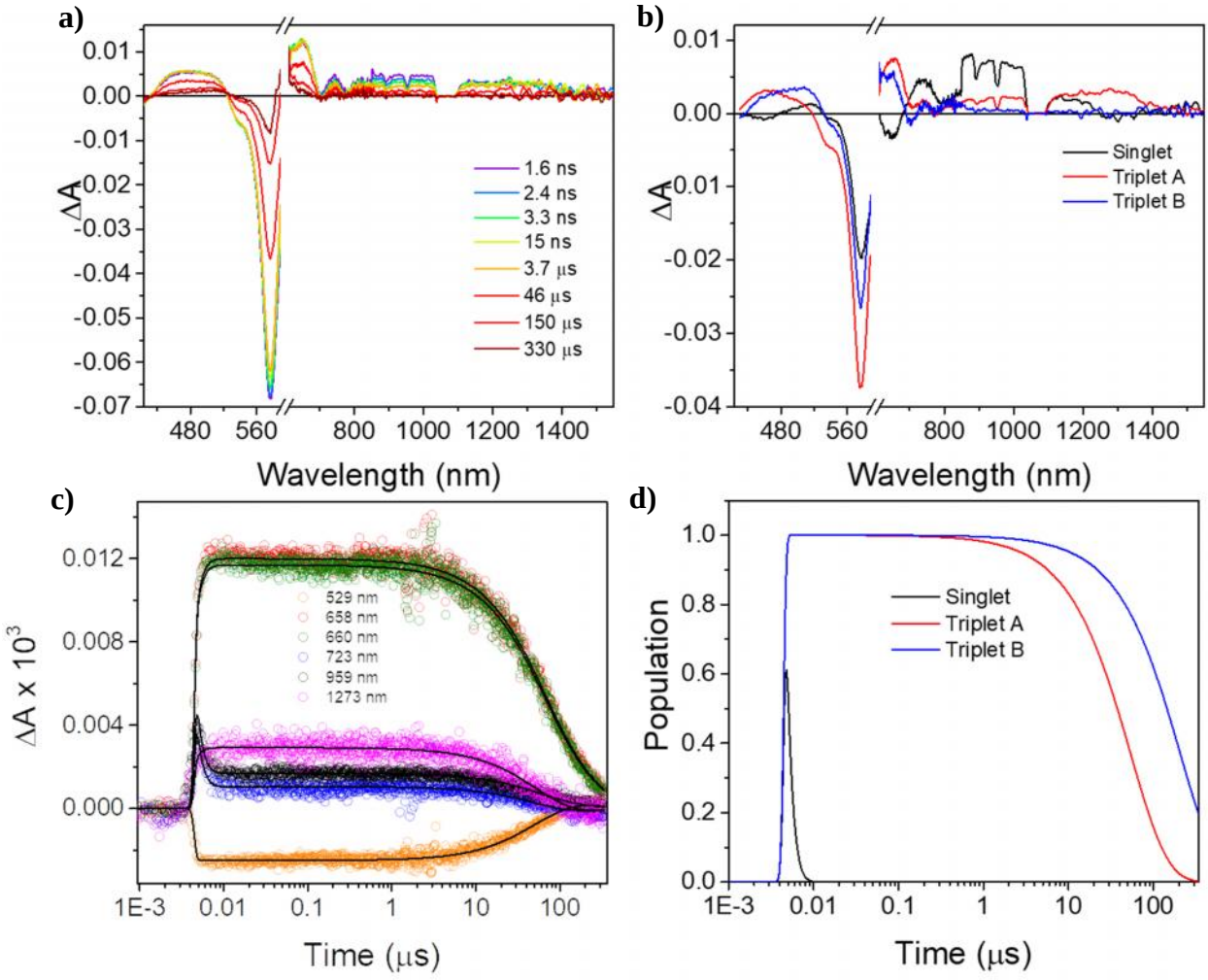

Figure S11. (a) fsTA spectra of **H_2-NDP** at selected time points and global fits: (b) decay-associated spectra using tri-exponential fit (c) wavelength fitting and (d) population vs. time plots.

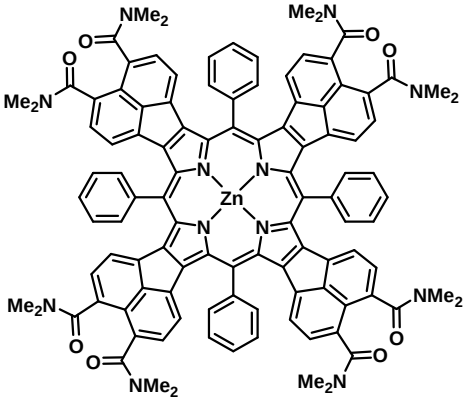

Zn-NDP

Zn–NDP

Upon photoexcitation of **Zn-NDP** in DCM using 580 nm (1 μJ/pulse), there is singlet excited state absorption (ESA) that spans from 380 nm to 1600 nm. In later time, there is triplet formation where the spectral feature is similar to singlet ESA except in the 1200 - 1600 nm region (Figure S11a). The fsTA spectra are globally fitted using A → B → C → GS where A is either higher lying singlet excited states ($S_n \leftarrow S_1$) or hot singlet excited state, B is relaxed singlet excited state and C is triplet. The relaxation from A to B has time constant of 2.7 ± 0.2 ps, and the effective relaxed singlet decay has time constant of 530 ± 10 ps and the triplet decay is longer than the time window of the experiment (>> 7.4 ns). The triplet decay is measured using timer window of 340 μs (Figure S12). Using the tri-exponential fit, the singlet decays within the IRF and triplet decays bi-exponentially with time constants of 77 ± 1 μs and 250 ± 10 μs.

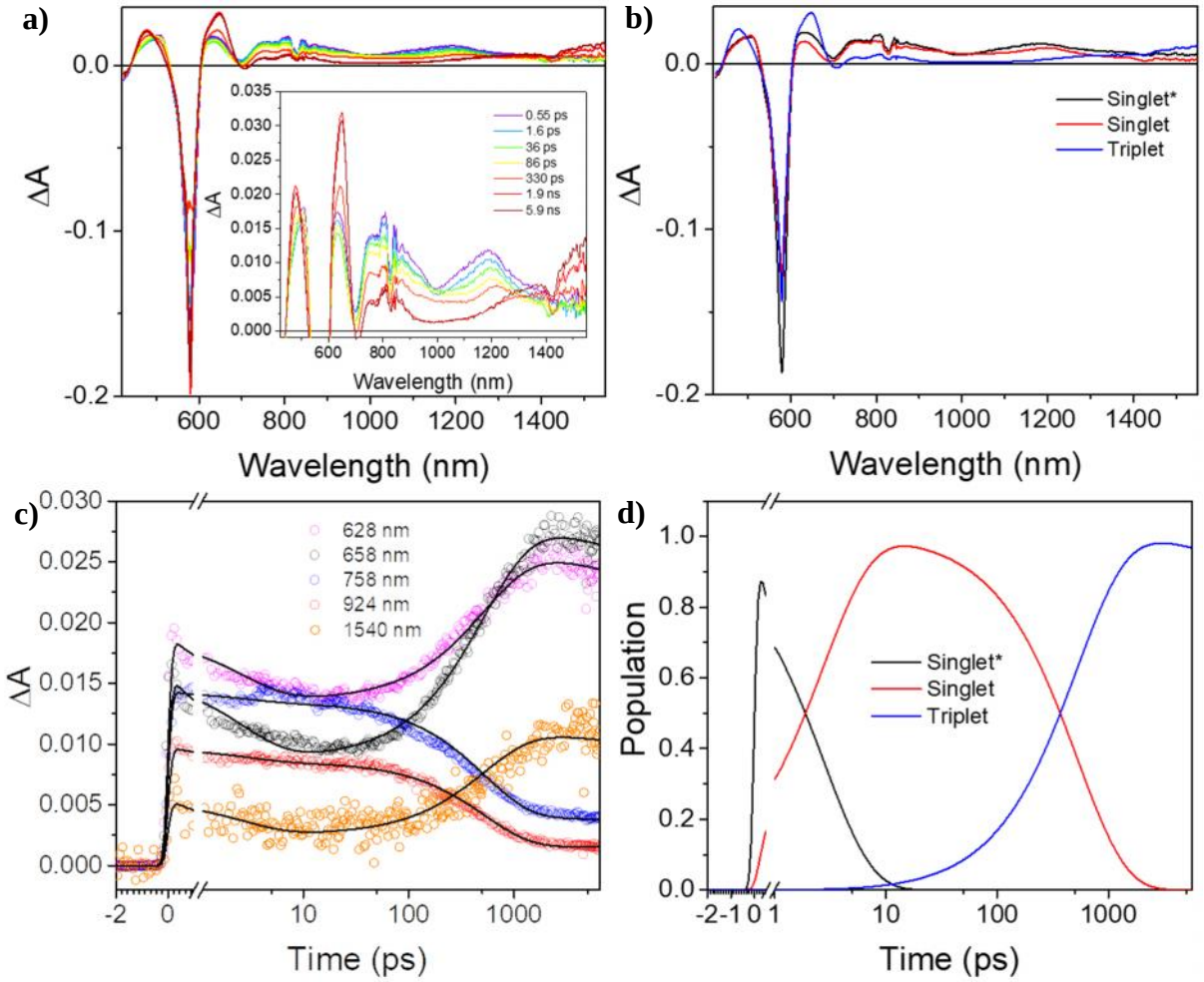

Figure S12. (a) fsTA spectra of **Zn-NDP** at selected time points with the inset showing the excited state abosorption features. (b) species-associated spectra using the kinetic A → B → C → GS where A is either higher lying singlet excited states ($S_n \leftarrow S_1$) or hot singlet excited state, B is relaxed singlet excited state and C is triplet. (c) wavelength fitting and (d) population vs. time plots.

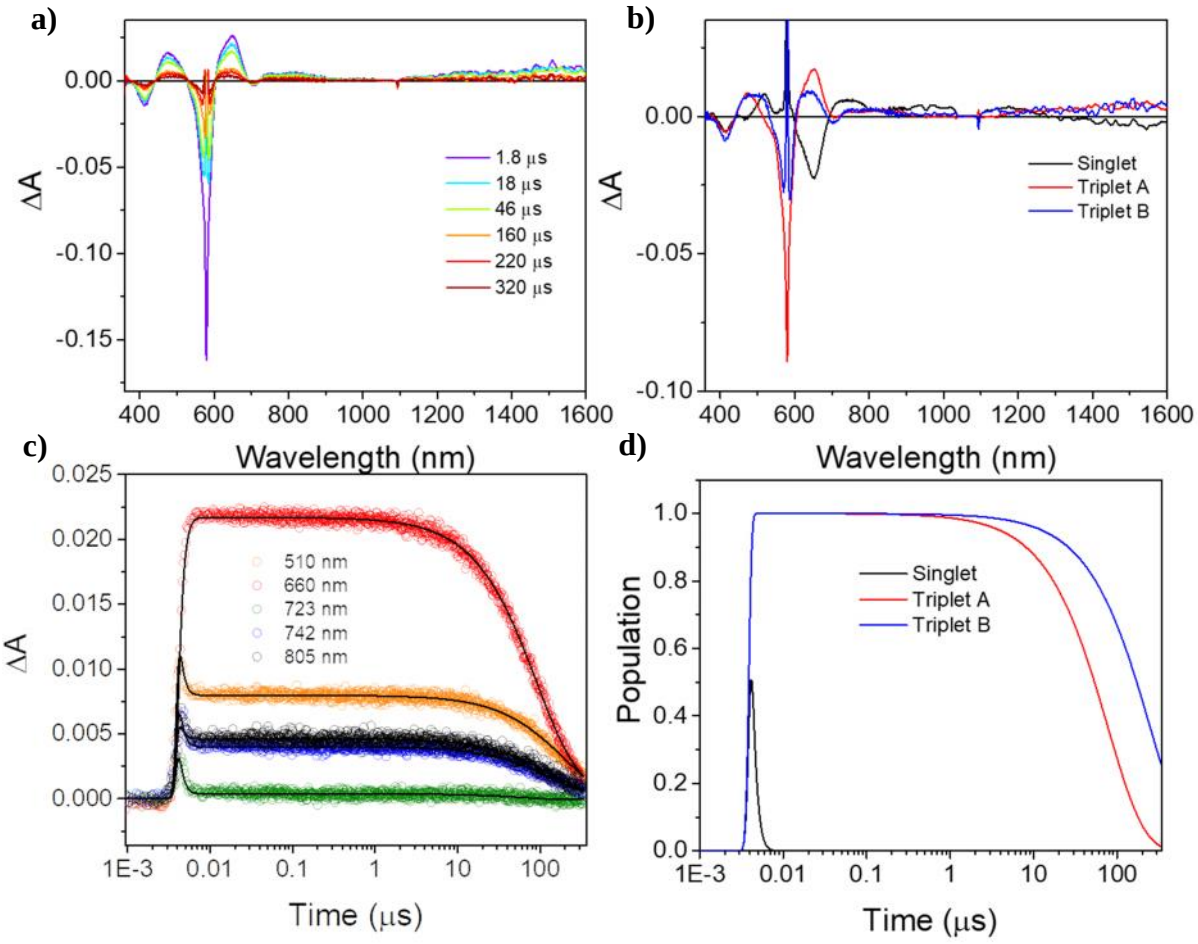

Figure S13. (a) fsTA spectra of **Zn-NDP** at selected time points and global fits: (b) decay-associated spectra using tri-exponential fit (c) wavelength fitting and (d) population vs. time plots.

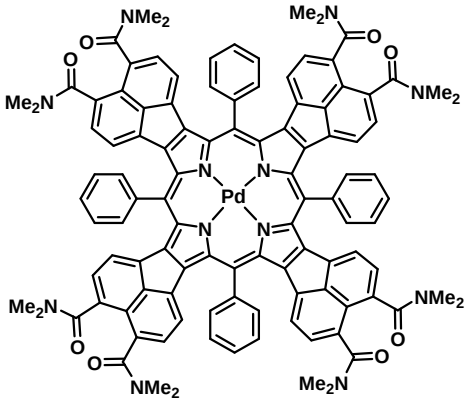

Pd-NDP

Pd–NDP.

Upon photoexcitation of **Pd- NDP** in air-free DCM using 540 nm (1 μJ/pulse), there is singlet excited state absorption (ESA) that spans from 380 nm to 1600 nm. In later time, there is triplet formation where the spectral feature is similar to the singlet ESA except in the 1450 nm region (Figure S13a). The effective singlet decay time constant (2.6 ± 0.1 ps) is obtained by globally fitting the fsTA spectra using A → B → GS where A is the singlet and B is the triplet. The triplet decay is measured using longer time window (Figure S14). The triplet decays bi-exponentially with time constants of 20 ± 1 μs and 52 ± 3 μs.

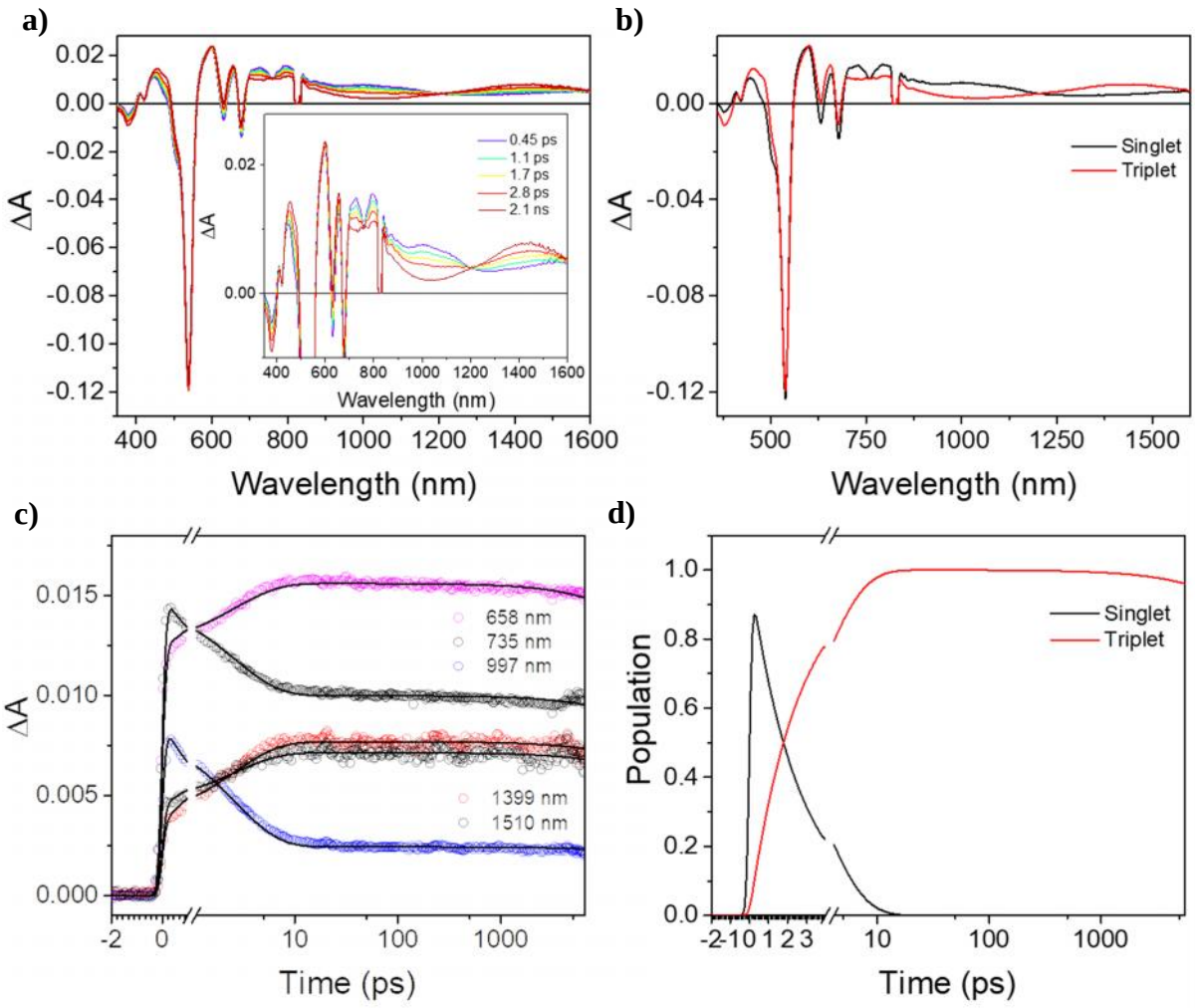

Figure S14. (a) fsTA spectra of **Pd-NDP** at selected time points with the inset showing the excited state absorption features. (b) species-associated spectra using the kinetic model A → B → GS where A is singlet and B is triplet. (c) wavelength fitting and (d) population vs. time plots.

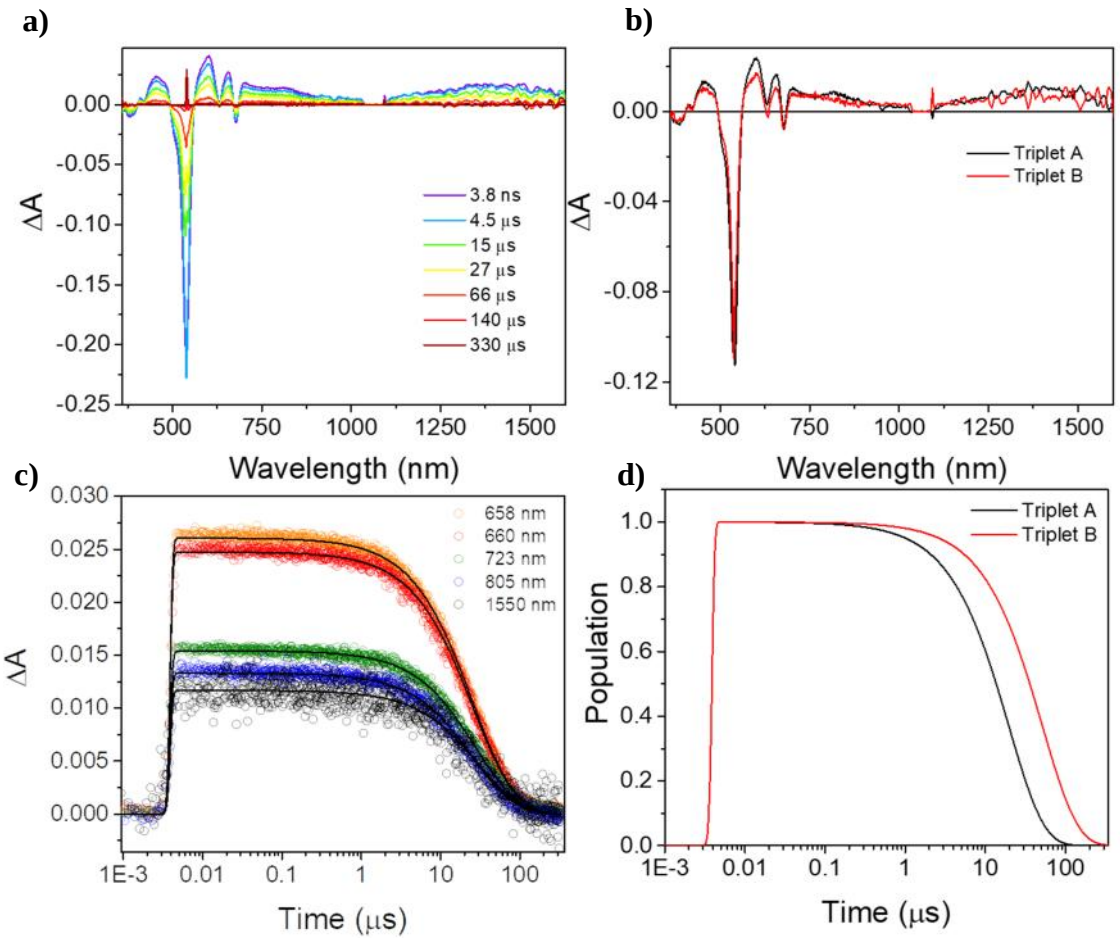

Figure S15. (a) fsTA spectra of **Pd-NDP** at selected time points and global fits: (b) decay-associated spectra using bi-exponential fit (c) wavelength fitting and (d) population vs. time plots.

Comparison

Comparing the triplet formation and decay rates among the three **M-NDPs**, **Pd-NDP** has the fastest triplet formation followed by **Zn-NDP** and **H_2-NDP** (Table S2). Similarly, triplet **Pd-NDP** has the fastest triplet decay time constants compared to **Zn-NDP** and **H_2-NDP**. The biexponential nature of triplet decay is some degree expected due to triplet-triplet annihilation. In fact, more concentrated **Pd-NDP** has faster triplet decays of 14 ± 1 μs and 42 ± 2 μs.

3 Theoretical Calculations

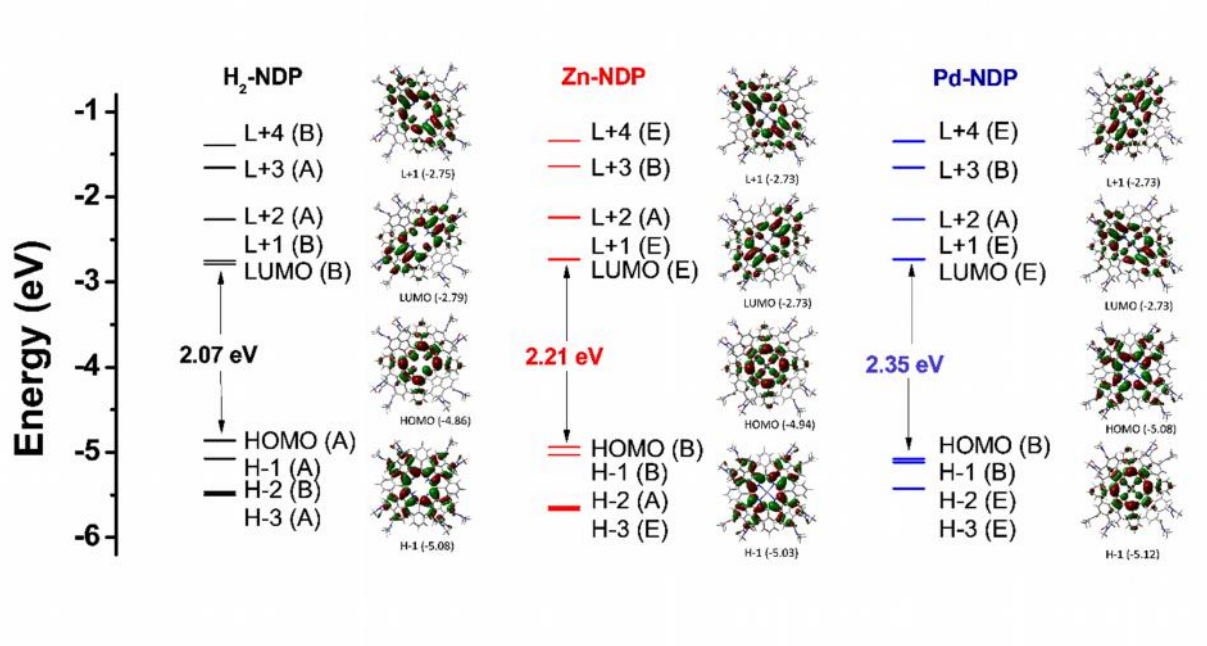

Figure S16. Kohn–Sham frontier molecular orbitals of **H_2-NDP** (black), **Zn-NDP** (red) and **Pd-NDP** (blue) calculated at B3LYP/6-31G(d,p) level of theory. In parentheses, all symmetries of MOs are denoted based on C2 (**H_2-NDP**) and S4 (**Zn-NDP** and **Pd-NDP**) point group.

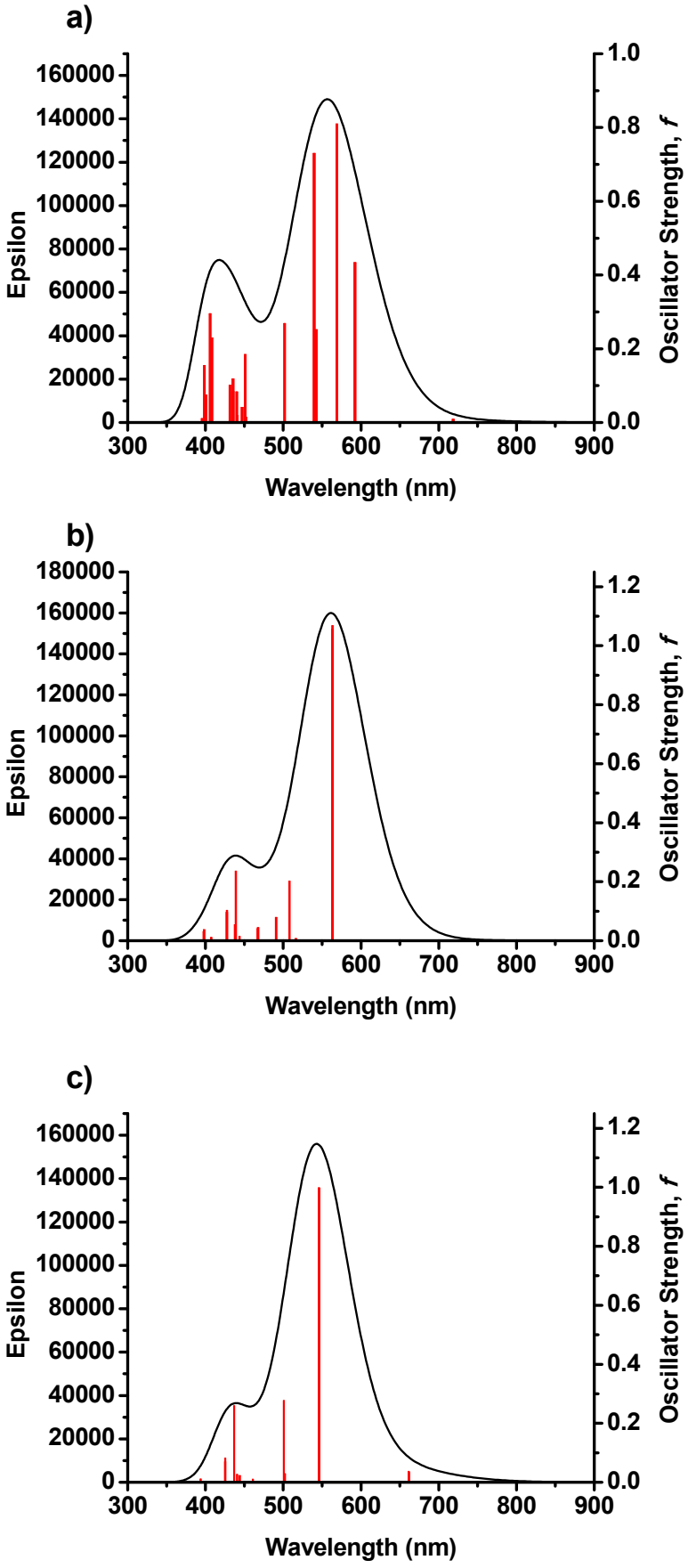

Figure S17. Time-dependent DFT electronic spectrum of a) **H_2-NDP**, b) **Zn-NDP** and c) **Pd-NDP** at B3LYP/6-31G(d,p) level of theory.

4. Photobiological Studies

Staphylococcus aureus 3150/12 was maintained on lysogeny broth (LB) broth agar and stored at 4 C. A single isolated colony was picked from this plate, transferred in 3 ml LB broth and incubated aerobically at 37 °C overnight in a rotary incubator with shaking at 180 rpm (rotations per minute). On the next day the bacteria were suspended in 20 ml of fresh LB medium to an optical density (OD_{600}) of 0.1 and grown in a flask to an attenuance of ca. OD_{600}=0.4. The bacterial suspension was then centrifuged at 4000 rpm for 5 min, resuspended in PBS to the final bacterial concentration of ca. $1x10^8$ cells per mL and subsequently used for the experiments.
Aqueous solutions of photosensitizers were prepared by first dissolving corresponding Por in a drop of dimethylsulfoxide (DMSO) and diluted using millipore water to the desired concentration. The final volume of DMSO was <1% of the total.

4.1 Photoinactivation of bacterial cells in planktonic cultures

To induce $^1O_2$ generation the 1 ml PS stained bacteria (15 min, 37 °C) were placed in 24-well plate and were irradiated using a projector lamp passing through a cut-off filter at 515 nm from the top of the plate. Fluence rates were routinely measured using power meter (Solar Meter from Solartech). To test type I and type II mechanisms free radical scavengers D-mannitol (100mM) and sodium azide (100 mM) were used. After irradiation, the living bacterial cells were determined by serial dilutions of the bacterial suspension and plating on LB agar plates. The plates were incubated overnight at 37 °C and the number of CFU/mL was determined. As controls, PS treated bacteria were kept in the dark (dark control) and untreated bacteria were exposed to light (light control).

4.2 Live/Dead staining

Cells were treated in the same way as for the evaluation with CFU counting. Following irradiation, samples were incubated with LIVE/DEAD® bacterial viability staining kit (*BacLight™ Bacterial Viability Kit*, Invitrogen L13152) for 15 min according to manufacturer's instructions. A 10 µL aliquot of the mixture was added to glass slides and covered with a glass coverslip. Fluorescence images were taken with a Nikon Eclipse Ci microscope, (40 X magnification). Excitation at 480 nm and long pass filter were used.

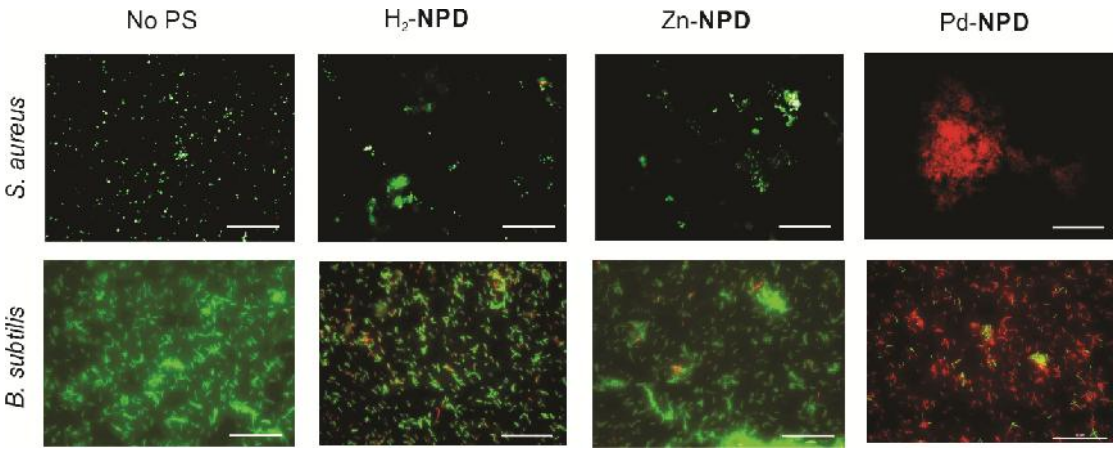

Figure S18. Representative fluorescence microscopy images of Live/Dead stained *S. aureus* and *B. subtilis* after incubation with H_2-**NDP**, Zn-**NDP** and Pd-**NDP** (15 min, 37°C) and irradiation with 9 J/cm^2 light doses. Scale bar 50µm.

References

1. H. Zhylitskaya, J. Cybińska, P. Chmielewski, T. Lis and M. Stępień, *J. Am. Chem. Soc.*, 2016, **138**, 11390–11398.
2. S. R. Greenfield, M. R. Wasielewski, *Opt. Lett.* 1995, **20**, 1394-1396.
3. R. M. Young, S. C. Jensen, K. Edme, Y. Wu, M. D. Krzyaniak, N. A. Vermeulen, E. J. Dale, J. F. Stoddart, E. A. Weiss, M. R. Wasielewski, D. T. Co, *J. Am. Chem. Soc.* 2016, **138**, 6163–6170.
4. Frisch, M. J.; Trucks, G. W.; Schlegel, H. B.; Scuseria, G. E.; Robb, M. A.; Cheeseman, J. R.; Scalmani, G.; Barone, V.; Mennucci, B.; Petersson, G. A.; Nakatsuji, H.; Caricato, M.; Li, X.; Hratchian, H. P.; Izmaylov, A. F.; Bloino, J.; Zheng, G.; Sonnenberg, J. L.; Hada, M.; Ehara, M.; Toyota, K.; Fukuda, R.; Hasegawa, J.; Ishida, M.; Nakajima, T.; Honda, Y.; Kitao, O.; Nakai, H.; Vreven, T.; Montgomery, Jr., J. A.; Peralta, J. E.; Ogliaro, F.; Bearpark, M.; Heyd, J. J.; Brothers, E.; Kudin, K. N.; Staroverov, V. N.; Kobayashi, R.; Normand, J.; Raghavachari, K.; Rendell, A.; Burant, J. C.; Iyengar, S. S.; Tomasi, J.; Cossi, M.; Rega, N.; Millam, J. M.; Klene, M.; Knox, J. E.; Cross, J. B.; Bakken, V.; Adamo, C.; Jaramillo, J.; Gomperts, R.; Stratmann, R. E.; Yazyev, O.; Austin, A. J.; Cammi, R.; Pomelli, C.; Ochterski, J. W.; Martin, R. L.; Morokuma, K.; Zakrzewski, V. G.; Voth, G. A.; Salvador, P.; Dannenberg, J. J.; Dapprich, S.; Daniels, A. D.; Farkas, Ö.; Foresman, J. B.; Ortiz, J. V.; Cioslowski, J.; Fox, D. J. *Gaussian 09 Revision E.01;* Gaussian Inc.: Wallingford CT, 2009.
5. Becke, A. D. *Phys. Rev. A* **1988**, *38*, 3098–3100.
6. Becke, A. D. *J. Chem. Phys.* **1993**, *98*, 5648–5652.
7. Lee, C.; Yang, W.; Parr, R. G. *Phys. Rev. B* **1988**, *37*, 785–789.